ELSEVIER

Thermochimica Acta 378 (2001) 125–133

thermochimica acta

www.elsevier.com/locate/tca

A comparative study on the kinetics and mechanism for the formation of $R_2Ba_4Cu_6O_{13}$ (R = Y, La, Nd, Sm, Eu or Er) from citrate precursors using non-isothermal TG

S. Arul Antony[a], C. Mallika[b], V. Sridharan[b], K.S. Nagaraja[a], O.M. Sreedharan[b,*]

[a]*Department of Chemistry, Loyola College, Chennai 600 034, India*
[b]*Department of Atomic Energy, Metallurgy and Materials Group, Indira Gandhi Centre for Atomic Research, Kalpakkam 603 102, India*

Received 11 January 2001; accepted 30 May 2001

Abstract

The kinetics and mechanism of the two-step reactions occurring in the precursor powders for the formation of the $R_2Ba_4Cu_6O_{13}$ (R = Y, La, Nd, Sm, Eu or Er) by citrate-fire method were studied by employing dynamic TG at linear heating rates of 5, 10 and 20°C/min in static air. The two-step reaction sequence occurring in the precursors comprising essentially $R(OH)_3$ (or $RO(OH)/R_2O_3$), $BaCO_3$ and CuO were analyzed by the integral approach using 23 functional forms for $G(\alpha)$. In the case of Y or La bearing precursors, the first step leading to the partial formation of $BaCuO_2$ and $R_2Cu_2O_5$ followed PT^4 mechanism while the final weight loss of CO_2 corresponding to the formation of $R_2Ba_4Cu_6O_{13}$ followed the 1D diffusion. However, in the case of other lanthanides (Nd, Sm, Eu and Er) the mechanisms were found to be 2D diffusion for the first step (partial formation of $BaCuO_2$ and R_2CuO_4) and 3D diffusion for the final step corresponding to the loss of CO_2 from remaining $BaCO_3$ leading to the formation of $R_2Ba_4Cu_6O_{13}$.

Keywords: Non-isothermal kinetics; RBCO superconductor-reaction mechanism; Dynamic TG

1. Introduction

Thermoanalytical techniques were first employed by Gadalla and Hegg [1] for the study of formation of $Y_2Ba_4Cu_6O_{13}$ through sequential reactions in the mixture of Y_2O_3, $BaCO_3$ and CuO prepared by conventional ceramic route. Results of such comprehensive investigations were reported in the literature by Sestak and Koga [2] and others [3–6]. Following Blank et al. [7], Pankajavalli et al. [8] reported the synthesis of $Y_2Ba_4Cu_6O_{13}$ from the precursors obtained by citrate auto-combustion, in which precursors essentially comprised an intimate mixture of micron size Y_2O_3, $BaCO_3$ and CuO in the mole ratio 1:4:6. However, no attempt was made in the literature to make a comparative study of the kinetics and mechanism of reactions taking place in the citrate auto-combustion precursors of a group of rare earth elements including Y and La. Hence, this study was undertaken.

2. Experimental

2.1. Materials

R_2O_3 (R = Y, La, Nd, Sm, Eu or Er) with purity better than 99.99% (Indian Rare Earths), $BaCO_3$

* Corresponding author. Fax: +91-4114-40301.
E-mail address: oms@igcar.ernet.in (O.M. Sreedharan).

0040-6031/01/$ – see front matter
PII: S0040-6031(01)00588-3

(99.8%, Sarabhai–Merck, India) and CuO (99.9%, E-Merck, India) were used. Other chemicals such as nitric acid, citric acid and ammonia were of G.R. grade purity.

2.2. Procedure

Required quantities of R_2O_3, $BaCO_3$ and CuO were separately dissolved in a small excess of 1:4 HNO_3 followed by mixing with a solution of citric acid, the number of moles of which is seven times that of R. Subsequently, the pH of the solution was adjusted to 6.8 by drop wise addition of ammonia. The resultant mixture was viscous and deep blue in color. It was slowly evaporated in a beaker, whose volume was more than 10 times that of the syrupy liquid. During evaporation there was no solid segregation. Prior to the spontaneous flame-up of this mixture the homogeneous solution swelled into a foam of fine flakes which nearly filled the entire vessel when the fire was triggered by self-ignition of ammonium nitrate. Before the onset of fire, the beaker was covered with a long stem inverted funnel to prevent the escape of finely divided particles. The quantity of each of the six precursors was limited to 5 g or less in order to limit the temperature rise caused by the fire to be within 400°C and the temperature was monitored with the fast response thermocouple dipped in the syrupy liquid during heating. When larger quantities were produced the temperature exceeded even 700°C resulting in larger particle sizes besides partial completion of reaction which were intended to be studied.

For carrying out the TG runs, the precursor powders were individually compacted into pellets of 6 mm diameter and 2–3 mm thickness at a pressure of 100 MPa. Pieces of these pellets were used for TG runs recorded at heating rates of 5, 10 and 20°C/min in static air using a horizontal thermoanalyzer Model Seiko-320.

Small fractions (about 20%) of these precursors were subjected to annealing in pure oxygen by gradual heating to the maximum temperature in the range 850–1000°C followed by controlled rates of cooling in flowing oxygen in different isothermal steps in order to achieve the oxygen stoichiometry in excess of $RBa_2Cu_3O_{6.9}$ required for superconductivity. The maximum and the intermediate temperatures of oxygen annealing as well as the rates of heating and cooling somewhat differed from one rare earth product to another. The fully oxygen annealed samples were essentially used to ascertain the formation of $RBa_2Cu_3O_{7-x}$ phases free from impurities to the extent detectable by powder X-ray diffraction (XRD) and critical temperature (T_c) measurements using magnetic susceptibility. Complete wet chemical analysis of not only oxygen stoichiometry, but also of the cations R, Ba and Cu were carried out before and after oxygen annealing. The cation stoichiometries in particular were found to differ negligibly from the designated formulae. The details of cation analyses and the XRD and O/M characterization studies following oxygen annealing were presented elsewhere [9].

Some of the TG runs were repeated up to a temperature by which the first step of reaction was complete so as to generate samples for phase analysis by XRD. Exposure of the precursor products as well as those quenched after the first step of the reaction to the ambient atmosphere could not be avoided which might have resulted in moisture pick-up. Matlab programs were used for the processing of regression data accrued from the non-isothermal TG runs on the six precursor samples.

3. Results and discussion

The XRD pattern taken for the Eu bearing sample in three different stages, namely as precursor powder, as a product obtained upon heating to 700°C at a linear heating rate of 10°C/min and as the final product of $EuBa_2Cu_3O_{7-x}$ after completion of oxygen annealing steps are shown in Fig. 1. The lattice parameters for the orthorhombic unit cell of $EuBa_2Cu_3O_{7-x}$ were found to be $a = 385.45$, $b = 389.01$ and $c = 1171$ pm and the cell volume $V = 0.1756$ $(nm)^3$ in good agreement with the values of $a = 385.1$, $b = 390.4$ and $c = 1169$ pm and the cell volume $V = 0.1757$ $(nm)^3$ reported in the literature [10]. The lattice parameters of the other five analogs were reported elsewhere [9]. Similar patterns were taken for other samples, but are not shown here for the sake of brevity.

The results of electro-gravimetric determination of Cu and two-stage complexometric determination of Ba and R as well as iodometric analyses of O/M ratios of the fully reacted precursors before and after the final

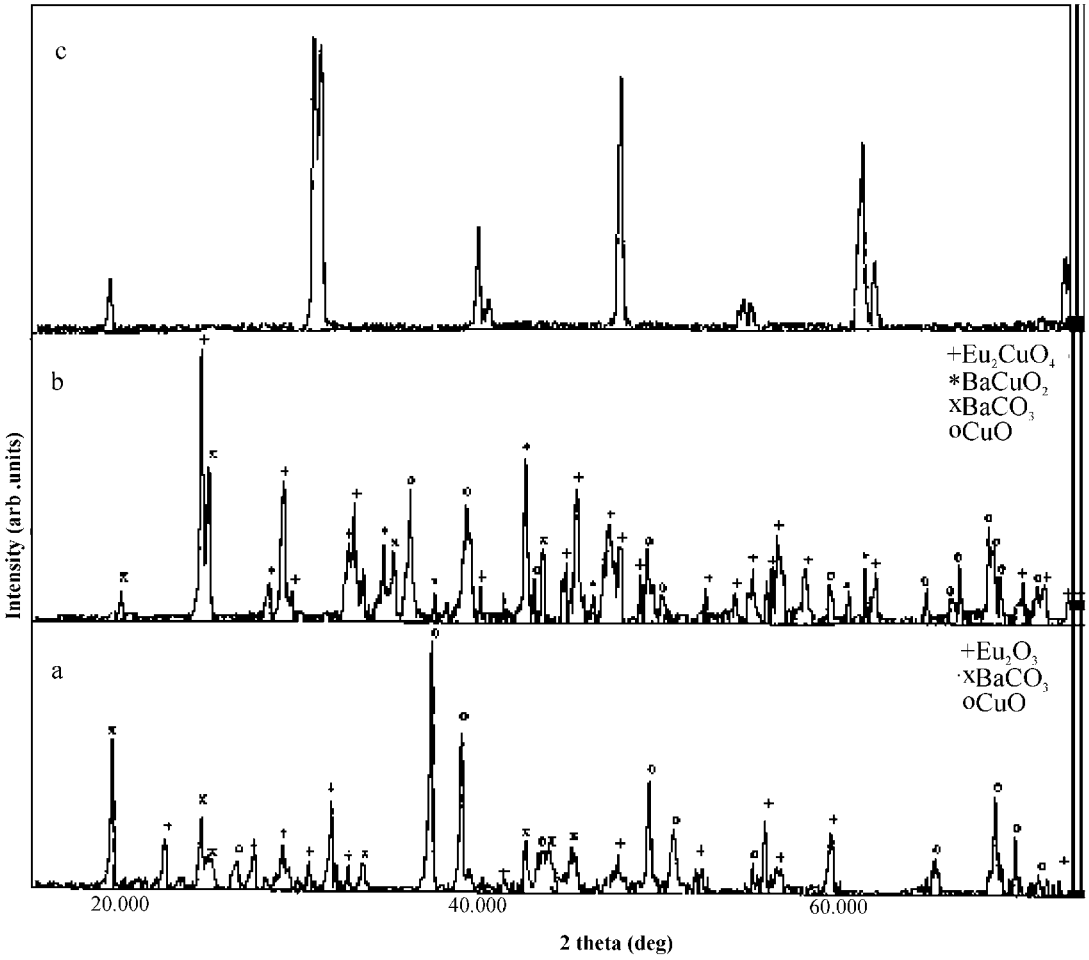

Fig. 1. XRD pattern of $EuBa_2Cu_3O_{7-x}$ after: (a) spontaneous citrate combustion; (b) the lower temperature reaction of the precursor upon heating it in air at 700°C; (c) completion of annealing at 950°C.

oxygen annealing reported elsewhere [9] are referred to here for asserting the conformity of the cation stoichiometries to within 1% of the stated formulae. The final products after complete oxygen annealing were found to be superconducting phases as seen by magnetic susceptibility measurements. A typical plot of magnetic susceptibility of Eu-123 obtained from the precursor is shown in Fig. 2.

A major part of this investigation was aimed at elucidating the kinetics and mechanism of the two reaction steps, taking place in the precursor powders, by employing dynamic TG and to make a comparison among the different rare-earth analogs. With this objective, the TG curves recorded for the six different citrate-fire precursors, in static air, at a linear heating rate of 10°C/min is shown in Fig. 3 (after normalizing the sample weights for representation as a single plot). Similar TG plots were recorded for two other linear rates of heating, namely 5 and 20°C/min, but are not presented here to avoid redundancy owing to the similarities in their shapes and trends in the TG curves obtained from the same set of precursor samples.

The analysis of the TG results represented in Fig. 3 were carried out on the basis of the following observations and inferences:

1. All the TG traces clearly show the occurrence of the reactions in two steps with the first step ending

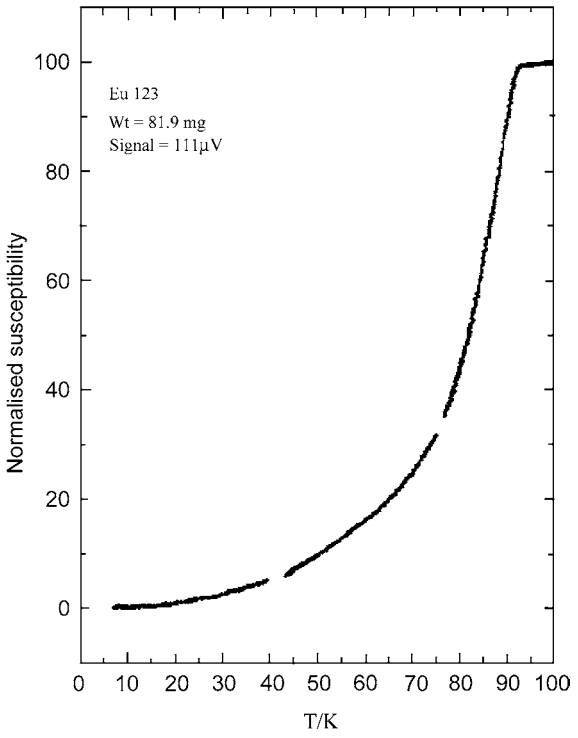

Fig. 2. A typical susceptibility–temperature plot for Eu-123 sample after the final treatment.

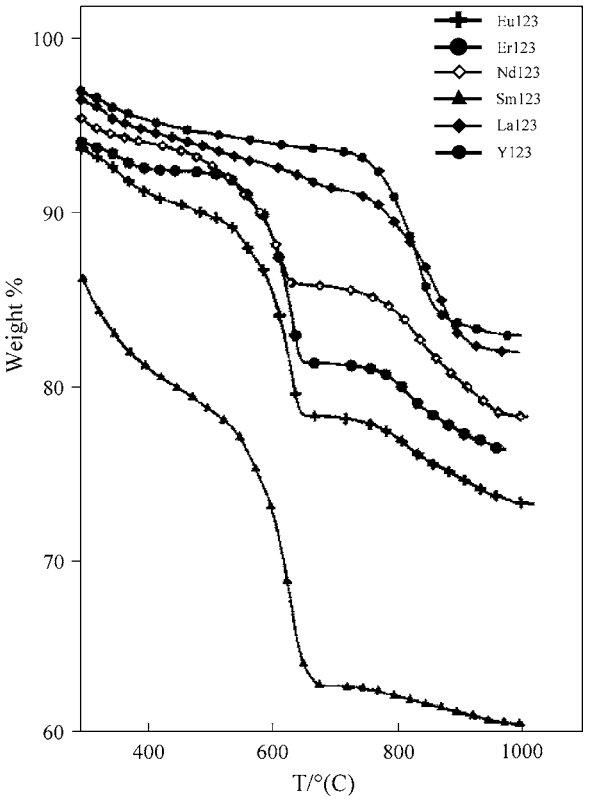

Fig. 3. Experimental results of TG analysis of citrate precursors for R-123 (R = Y, La, Nd, Sm, Eu, or Er) in static air at a heating rate of 10°C/min.

by about 650–700°C and the second by about 970–1010°C.

2. The products at the end of the second step were $R_2Ba_4Cu_6O_{13}$ as reported earlier.
3. The only weight loss in the second step was assumed to be due to the evolution of CO_2 as a consequence of the higher temperature reaction (Table 3, Column 2) involving $BaCO_3$ (left over after the first step) leading to the stoichiometry given under the observation (2). When the final weight of the sample after the higher temperature reaction was normalized to 1 mole of R, by subtracting the number of moles of $BaCO_3$ taking part in higher temperature reaction, the number of moles of Ba existing as $BaCuO_2$ and $BaCO_3$ were back calculated.
4. The starting point of the first step was taken to be that temperature at which all the organics were oxidized and the samples were free from adsorbed moisture/water of hydration, if any. The weight loss in the lower temperature reaction was attributed not only to partial weight loss in $BaCO_3$ (forming $BaCuO_2$), but also to H_2O loss from hydroxides/oxy-hydroxide. The relative amounts of $BaCO_3$ and the rare earth hydroxide/oxy-hydroxide were arrived at by matching the calculated weight losses of CO_2 and H_2O with the observed values.
5. After initial drying and combustion of organics, the Y precursor was assumed to comprise Y_2O_3, $BaCO_3$ and CuO and no trace of $Y(OH)_3$, YO(OH) or $Y(OH)CO_3$ was assumed to be present. This assumption is consistent with the XRD analysis as well as the observation reported by Pankajavalli et al. [8] on the thermal decomposition of hydrated yttrium carbonate which was found to be complete by 310°C. The lanthanides Sm, Eu and Er were present as $R(OH)_3$, whereas La and Nd were present as RO(OH) as per our phase analysis and

in agreement with the temperature ranges of decomposition of rare earth hydroxides and oxyhydroxides reported in the literature [11,12].

Thus the partial reactions occurring in the higher temperature region of 720–1010°C were first computed from the weight loss taken as that due to CO_2 evolution and are listed in Column 2 of Table 3, followed by the identification of the partial reaction in the lower temperature step as in Column 2 of Table 1. It should be pointed out that the TG results from the lower temperature step is presented first even though the weight loss analyses commenced from the final weight losses.

The integral method [1,2,13–16] was used in analyzing the data to identify the probable mechanism and to compute the kinetic parameters. At this juncture, it should be borne in mind that the lower temperature step involved at least two parallel reactions, one of which leading to partial $R_2Cu_2O_5$ or R_2CuO_4, formation while the other to the partial formation of $BaCuO_2$. Likewise, the final step also involved parallel reactions between the rare earth copper interoxide and $BaCuO_2$ as well as with unreacted portions of $BaCO_3$ and CuO. Thus, fitting of the kinetics of the two steps with parametric expressions would give rise to only average values of activation energies and pre-exponential factors and not those specific to any particular reaction. In short, these values should be taken more as curve fitting constants and the mechanisms also would reflect the averaged pathways of reactions in the respective steps. In the integral approach, the following equation was employed:

$$\ln\left[\frac{G(\alpha)}{T^{1.92150}}\right] = \ln\left(\frac{AE_a}{\beta R}\right) + 3.77205 - 1.92150\ln E_a - \frac{E_a}{RT} \quad (1)$$

where E_a= activation energy = slope × R; A= exp (intercept $-3.77205 + 1.92150\ln E_a$) × $\beta R/E_a$; β the heating rate; A the frequency factor; α the fraction of conversion and $G(\alpha)$ is the most probable mechanism function. $G(\alpha)$ was arrived at by analyzing the data with 23 different functional forms such as the ones corresponding to power and exponential laws, 1D, 2D or 3D diffusion, Prout–Thompkins, Avrami–Erofeev, and Ginstling–Brouns which were listed by many workers including Gao and Dollimore [13].

The results of TG experiments such as the ones shown in Fig. 3 for a given heating rate namely, 10°C/min, were transformed into plots of fraction reacted (α) against temperature for all the six precursors at three different heating rates. Representing all the 18 such plots would be unwieldy. Hence, typical $\alpha-T$

Table 1
Thermoanalytical characterization of lower temperature (400–710°C) reaction in R-123 citrate precursors: TG characterization

R	Reaction	Heating rate (°C/min)	Weight change	
			Observed (%)	Calculated (%)
Y	$Y_2O_3 + 0.3BaCO_3 + 2.3CuO \rightarrow$	5	2.78	2.97
	$Y_2Cu_2O_5 + 0.3BaCuO_2 + 0.3CO_2\uparrow$	10	3.10	2.97
		20	2.96	2.97
La	$La_2O_2(OH)_2 + 0.2BaCO_3 + 2.2CuO \rightarrow$	5	4.58	4.79
	$La_2Cu_2O_5 + 0.2BaCuO_2 + 0.2CO_2\uparrow + H_2O$	10	4.66	4.80
		20	4.72	4.80
Nd	$Nd_2O_2(OH)_2 + 1.1BaCO_3 + 2.2CuO \rightarrow$	5	8.86	8.94
	$Nd_2CuO_4 + 1.1BaCuO_2 + 1.1CO_2\uparrow + H_2O$	10	8.92	8.94
		20	9.00	8.94
Sm	$Sm_2(OH)_6 + 2.8BaCO_3 + 3.8CuO \rightarrow$	5	14.49	14.09
	$Sm_2CuO_4 + 2.8BaCuO_2 + 2.8CO_2\uparrow + 3H_2O$	10	13.89	14.09
		20	14.49	14.09
Eu	$Eu_2(OH)_6 + 1.7BaCO_3 + 2.7CuO \rightarrow$	5	13.91	13.87
	$Eu_2CuO_4 + 1.7BaCuO_2 + 1.7CO_2\uparrow + 3H_2O$	10	13.95	13.87
		20	14.01	13.87
Er	$Er_2(OH)_6 + 1.8BaCO_3 + 2.8CuO \rightarrow$	5	13.22	13.38
	$Er_2CuO_4 + 1.8BaCuO_2 + 1.8CO_2\uparrow + 3H_2O$	10	13.42	13.38
		20	13.31	13.38

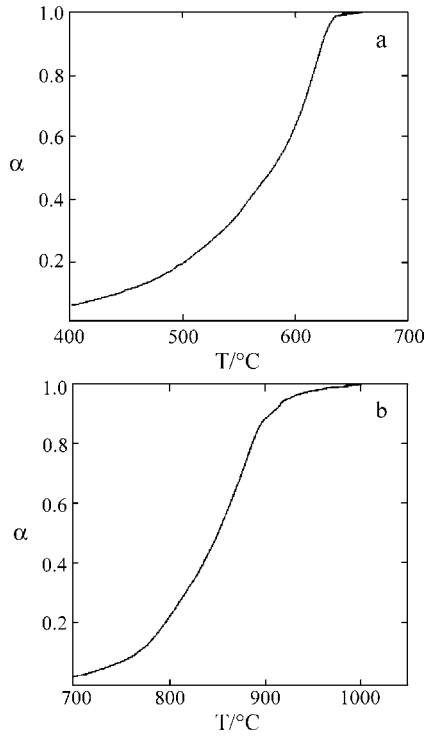

Fig. 4. Typical $\alpha-T$ plots for: (a) La sample (lower temperature) and (b) Er sample (higher temperature).

plots for La and Er precursors at a heating rate of 5°C/min are shown in Fig. 4. The rationale for the choice of La and Er precursors out of the six sets is that La as well as Y, and Er as well as other three lanthanide precursors follow two different sets of mechanism, respectively, for the two steps of the reaction sequence (as will be evident from the later section).

By testing each of the 18 $\alpha-T$ curves such as the one shown in Fig. 4 with the 23 functional forms of $G(\alpha)$, the one which yielded the best straight line representation was chosen as the valid $G(\alpha)$ function. Thus, for the lower temperature reaction, the mechanism was identified to be the PT^4 for Y and La precursors while one-dimensional diffusion should be operative in the case of the other four rare earths (cf. Table 2). However, for the higher temperature (step 2) reaction, two-dimensional and three-dimensional diffusion mechanisms were found to be valid for Y/La and the other four rare earth precursors, respectively (cf. Table 4). These $G(\alpha)$ plots are shown in Figs. 5 and 6 for La and Er analogs for the two steps of the reaction sequence.

The values of standard deviations S_{xy} and S_b and correlation coefficient (r) for the two steps are also listed in Tables 1–4, the values of which facilitate

Table 2
Thermoanalytical characterization of lower temperature (400–710°C) reaction in R-123 citrate precursors: regression analysis of mechanism and kinetic parameters

R	Exact T range (°C)	Mechanism	Correlation factor	E_a (kJ/mol)	A	S_{xy}	S_b
Y	383.1–693.0	PT^{4a}	0.9922	103.6	2.02×10^6	5.5×10^{-4}	0.978
	353.1–693.6		0.9913	99.5	1.28×10^6	1.8×10^{-4}	1.887
	347.9–663.2		0.9973	85.0	1.28×10^6	1.8×10^{-4}	0.384
La	375.9–703.5	PT^4	0.9980	192.2	1.17×10^9	5.1×10^{-4}	0.959
	370.6–693.0		0.9987	181.6	7.55×10^8	4.7×10^{-4}	0.998
	383.5–715.8		0.9982	161.1	4.30×10^7	6.6×10^{-4}	1.375
Nd	396.9–693.2	1D[b]	0.9991	147.1	5.12×10^5	6.4×10^{-5}	0.348
	380.8–673.0		0.9985	129.4	6.36×10^4	7.6×10^{-5}	0.366
	380.6–690.5		0.9986	118.3	1.75×10^4	5.2×10^{-5}	0.213
Sm	420.2–693.5	1D	0.9969	182.0	3.98×10^7	2.5×10^{-4}	1.697
	393.1–703.3		0.9965	189.1	1.03×10^8	2.7×10^{-4}	2.066
	413.3–708.4		0.9967	179.6	3.17×10^7	2.3×10^{-4}	1.564
Eu	350.0–683.0	1D	0.9947	218.8	6.34×10^9	4.9×10^{-4}	3.772
	345.2–693.0		0.9998	209.5	2.04×10^9	4.6×10^{-4}	3.947
	355.4–703.5		0.9936	171.9	1.42×10^7	1.9×10^{-4}	0.887
Er	390.0–702.0	1D	0.9989	324.2	1.0×10^{16}	1.7×10^{-4}	2.378
	398.0–708.0		0.9979	283.3	6.8×10^{16}	8.9×10^{-4}	5.811
	418.0–708.0		0.9967	259.2	6.5×10^{11}	3.8×10^{-4}	0.272

[a] Prout-Thompkins branching of nuclei.
[b] One-dimensional diffusion.

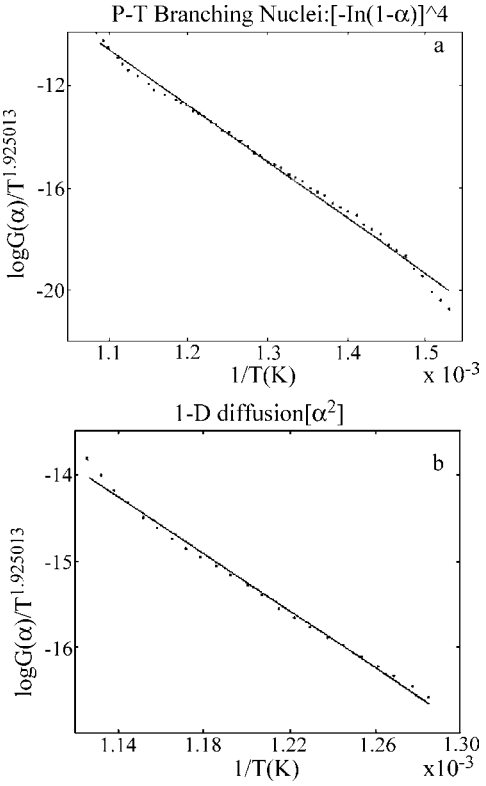

Fig. 5. Regression plots for the lower temperature step for: (a) La and (b) Er bearing samples.

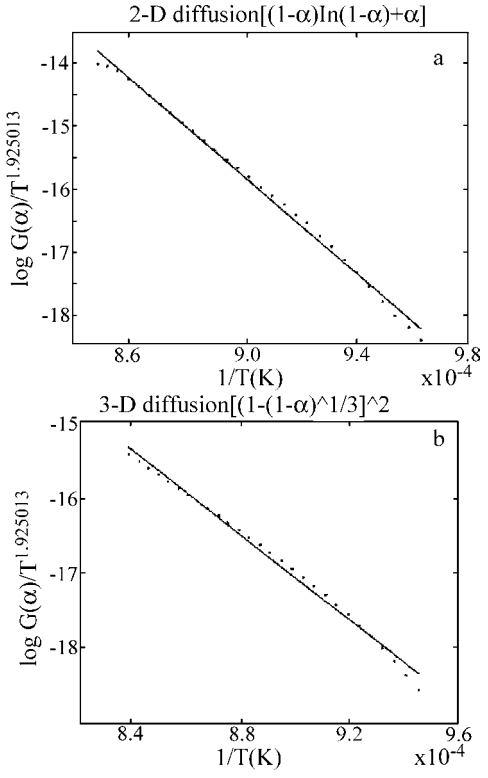

Fig. 6. Regression plots for the higher temperature step for: (a) La and (b) Er bearing samples.

testing the linearity. For instance, the nearer the value of r to unity and smaller the two standard deviations, better would be the linearity which in essence is the criterion for the choice of the mechanism. The tables also summarize the values of activation energy and the pre-exponential factors calculated from Eq. (1). These parameters should be taken more as curve fitting constants for each of the two reaction steps for the respective precursors. The first step could be associated with the partial reactions leading to the formation of $BaCuO_2$ and either R_2CuO_4 (R = Nd, Sm, Eu or Er) or $R_2Cu_2O_5$ (R = Y or La) and the second step involved the reaction with the major part of $BaCO_3$ unconsumed in the first step. The DTA simultaneously recorded was quite complicated with overlapping peaks which could help to identify only two broad reaction endotherms. However, endotherm corresponding to the phase transition in $BaCO_3$ at 813°C was found to be qualitatively proportional to its quantity indicated as participating in the second step of the reaction sequence. After the termination of the heating cycle, no detectable DTA peak could be observed around 813°C during the re-heating cycle indicating the absence of any residual $BaCO_3$.

The three-dimensional diffusion mechanism observed for the second step in the case of lanthanides and two-dimensional diffusion for the other two rare earths are in agreement with those reported in the literature wherein the gel type methods were employed for the synthesis of the precursors. For step 2, the pre-exponential factor (A, which is in the range of 10^{13}–10^{18}) is several orders of magnitude greater than those for the first step of reaction. This is understandable in view of the growth in the particle size with temperature so that much larger particles could be associated with higher temperature step (and hence much higher magnitudes of A) as compared to those for the lower temperature step.

Table 3
Thermoanalytical characterization of higher temperature (680–1010°C) reaction in R-123 citrate precursors: TG characterization

R	Reaction	Heating rate (°C/min)	Weight change	
			Observed (%)	Calculated (%)
Y	$Y_2Cu_2O_5 + 3.7BaCO_3 + 0.3BaCuO_2 + 3.7CuO \rightarrow$	5	11.81	12.02
	$Y_2Ba_4Cu_6O_{13} + 3.7CO_2\uparrow$	10	11.99	12.02
		20	11.88	12.02
La	$La_2Cu_2O_5 + 3.8BaCO_3 + 0.2BaCuO_2 + 3.8CuO \rightarrow$	5	10.41	10.56
	$La_2Ba_4Cu_6O_{13} + 3.8CO_2\uparrow$	10	10.40	10.56
		20	10.29	10.56
Nd	$Nd_2CuO_4 + 2.9BaCO_3 + 1.1BaCuO_2 + 3.9CuO \rightarrow$	5	8.86	8.75
	$Nd_2Ba_4Cu_6O_{13} + 2.9CO_2\uparrow$	10	9.09	8.75
		20	8.96	8.75
Sm	$Sm_2CuO_4 + 1.2BaCO_3 + 2.8BaCuO_2 + 2.2CuO \rightarrow$	5	3.65	3.56
	$Sm_2Ba_4Cu_6O_{13} + 1.2CO_2\uparrow$	10	3.56	3.56
		20	3.28	3.56
Eu	$Eu_2CuO_4 + 2.3BaCO_3 + 1.7BaCuO_2 + 3.3CuO \rightarrow$	5	6.65	6.55
	$Eu_2Ba_4Cu_6O_{13} + 2.3CO_2\uparrow$	10	6.14	6.55
		20	6.55	6.55
Er	$Er_2CuO_4 + 2.2BaCO_3 + 1.8BaCuO_2 + 3.2CuO \rightarrow$	5	6.14	6.13
	$Er_2Ba_4Cu_6O_{13} + 2.2CO_2\uparrow$	10	6.31	6.13
		20	6.30	6.13

A somewhat systematic decrease in the apparent activation energy could be seen in the group of lanthanides with the exception of Eu for step 1. Likewise, larger apparent activation energies were associated with step 2 wherein larger quantities of $BaCO_3$ were involved in the reaction again with the exception of Er. One main observation made here is that the citrate-fire precursors are more reactive than those

Table 4
Thermoanalytical characterization of higher temperature (680–1010°C) reaction in R-123 citrate precursors: regression analysis of mechanism and kinetic parameters

R	Exact T range (°C)	Mechanism	Correlation factor	E_a (kJ/mol)	Frequency factor (A)	S_{xy}	S_b
Y	690.0–995.5	2D[a]	0.9994	445	7.94×10^{17}	9.2×10^{-5}	1.64
	690.6–996.1		0.9986	368	8.27×10^{13}	1.5×10^{-4}	1.92
	680.2–1012.4		0.9998	418	1.90×10^{16}	1.7×10^{-5}	0.24
La	973.5–1000.3	2D	0.9947	334	1.35×10^{12}	2.7×10^{-5}	0.31
	963.0–1000.3		0.9997	380	1.84×10^{15}	4.1×10^{-5}	0.52
	988.8–993.5		0.9998	325	1.44×10^{11}	1.4×10^{-5}	0.14
Nd	963.2–1010.3	3D[b]	0.9987	284	1.19×10^{9}	1.1×10^{-2}	0.80
	933.0–1010.6		0.9962	302	1.01×10^{10}	5.2×10^{-4}	0.50
	963.5–1010.5		0.9987	375	1.75×10^{13}	1.5×10^{-4}	1.48
Sm	963.5–983.0	3D	0.9967	230	3.63×10^{6}	2.5×10^{-4}	1.48
	973.3–1000.5		0.9969	208	4.45×10^{5}	1.8×10^{-4}	0.87
	963.5–993.0		0.9938	299	1.22×10^{10}	5.9×10^{-4}	4.44
Eu	933.5–1010.0	3D	0.9986	408	2.03×10^{15}	2.9×10^{-4}	2.38
	973.3–1010.0		0.9971	809	9.78×10^{33}	2.7×10^{-2}	4.45
	963.5–1010.3		0.9994	194	1.94×10^{15}	1.5×10^{-5}	0.17
Er	972.0–975.0	3D	0.9982	197	1.87×10^{15}	6.1×10^{-5}	0.56
	978.0–990.0		0.9992	137	1.22×10^{13}	1.1×10^{-5}	0.13
	978.0–1006.5		0.9974	190	2.23×10^{15}	5.5×10^{-5}	0.88

[a] Two-dimensional diffusion.
[b] Three-dimensional diffusion.

prepared by conventional ceramic route reported by Gadalla and Hegg [1] with the inception temperatures being considerably lower. Further, step 1 could not be identified with the completion of formation of any intermediate phase, but could be associated with only partial reactions.

4. Conclusions

1. The citrate-fire precursors were found to be more reactive in forming R123 by present TG studies compared to the reactivity of the conventional ceramic precursors as reported in the literature. This was evidenced by lower inception temperatures of the final weight loss step leading to $R_2Ba_4Cu_6O_{13}$.
2. The citrate-fire precursors for Y and La followed PT^4 and 1D diffusion mechanisms for the first and second step, respectively. This is in contrast with the 2D and 3D mechanisms followed by lanthanide precursors (Nd, Sm, Eu and Er) for the first and the second stage of reaction sequence, respectively.
3. The much higher order of the pre-exponential factor for the second step in contrast to those for the first step are generally indicative of growth in the particle size while proceeding from first to the second step of the reaction sequence.

Acknowledgements

The authors are grateful to Rev. Fr. John Pragasam, Director, LIFE, Loyola College and to Dr. Baldev Raj, Director, MCRG, IGCAR and Dr. V.S. Raghunathan, Associate Director, MCG, IGCAR for their keen interest and constant encouragement throughout the course of this work. The first author is grateful to UGC Teacher Fellowship awarded under FIP (TFTNMD-176 IX Plan).

References

[1] A.M. Gadalla, T. Hegg, Thermochim. Acta 145 (1989) 149.
[2] J. Sestak, N. Koga, Thermochim. Acta 203 (1992) 321.
[3] N.L. Wu, V.C. Chang, Thermochim. Acta 203 (1992) 339.
[4] M. Kamimoto, Thermochim. Acta 174 (1991) 153.
[5] G.V. Rama Rao, P.V.S. Prasad, R.K.S. Raman, S. Venkadesan, S.L. Mannan, U.V. Varadaraju, Thermochim. Acta 230 (1993) 207.
[6] J.C.W. Chien, B.M. Gong, J.M. Madsen, R.B. Hillock, Phys. Rev. B 38 (1988) 11853.
[7] D.H.A. Blank, H. Kruidhof, J. Flokstra, J. Phys. D 21 (1988) 226.
[8] R. Pankajavalli, J. Janaki, O.M. Sreedharan, J.B. Gnanamoorthy, G.V.N. Rao, V.S. Sastry, M.P. Janawadkar, Y. Hariharan, T.S. Radhakrishnan, Physica C 156 (1988) 737.
[9] S. Arul Antony, S. Sahasranaman, K.S. Nagaraja, O.M. Sreedharan, Physica C 323 (1999) 115.
[10] M.A. Alario-Franco, E. Moran-Mignelez, R. Saez-Puche, F. Garcia-Alvarado, U. Amador, M. Barahona, F. Fernandez, M.T. Perez-Frias, J.L. Vicent, Mater. Res. Bull. 23 (1988) 313.
[11] L. Eyring (Ed.), Progress in the Science and Technology of the Rare Earth, Vol. 1, Oxford, Pergamon Press, 1964, p. 287.
[12] L. Eyring (Ed.), Progress in the Science and Technology of the Rare Earth, Vol. 3, Oxford, Pergamon Press, 1968, p. 453.
[13] X. Gao, D. Dollimore, Thermochim. Acta 215 (1993) 47.
[14] A.B. Phadnis, V.V. Deshpande, Thermochim. Acta 62 (1983) 361.
[15] P.M. Madhu Sudanan, K. Krishnan, K.N. Ninan, Thermochim. Acta 97 (1986) 189.
[16] J. Sestak, Thermochim. Acta 3 (1971) 1.